The Astrophysical Journal Letters, 902:L47 (7pp), 2020 October 20 https://doi.org/10.3847/2041-8213/abbd3f

Confirming the Explosive Outflow in G5.89 with ALMA

Luis A. Zapata[1], Paul T. P. Ho[2,3], Manuel Fernández-López[4], Estrella Guzmán Ccolque[4], Luis F. Rodríguez[1,5], José Reyes-Valdés[6], John Bally[7], Aina Palau[1], Masao Saito[8,9], Patricio Sanhueza[8,9], P. R. Rivera-Ortiz[10], and A. Rodríguez-González[11]

[1] Instituto de Radioastronomía y Astrofísica, Universidad Nacional Autónoma de México, P.O. Box 3-72, 58090, Morelia, Michoacán, Mexico
l.zapata@irya.unam.mx
[2] Academia Sinica Institute of Astronomy and Astrophysics, P.O. Box 23-141, Taipei, 10617, Taiwan
[3] East Asian Observatory, 666 N. A'ohoku Place, Hilo, HI 96720, USA
[4] Instituto Argentino de Radioastronomía (CCT-La Plata, CONICET; CICPBA), C.C. No. 5, 1894, Villa Elisa, Buenos Aires, Argentina
[5] Mesoamerican Centre for Theoretical Physics, Universidad Autónoma de Chiapas, Carretera Emiliano Zapata Km. 4 Real del Bosque, 29050 Tuxtla Gutiérrez, Chiapas, Mexico
[6] Centro de Investigación en Matemáticas Aplicadas, Universidad Autónoma de Coahuila, Camporredondo S/N, Saltillo, Coahuila, CP 25115, Mexico
[7] Astrophysical and Planetary Sciences Department University of Colorado, UCB 389, Boulder, CO 80309, USA
[8] National Astronomical Observatory of Japan, National Institutes of Natural Sciences, 2-21-1 Osawa, Mitaka, Tokyo 181-8588, Japan
[9] Department of Astronomical Science, SOKENDAI (The Graduate University for Advanced Studies), 2-21-1 Osawa, Mitaka, Tokyo 181-8588, Japan
[10] Univ. Grenoble Alpes, CNRS, Institut de Planétologie et d'Astrophysique de Grenoble (IPAG), F-38000 Grenoble, France
[11] Instituto de Ciencias Nucleares, Universidad Nacional Autónoma de México, Ap. 70-543, 04510 D.F., Mexico
Received 2020 September 7; revised 2020 September 24; accepted 2020 September 28; published 2020 October 22

Abstract

The explosive molecular outflow detected decades ago in the Orion BN/KL region of massive star formation was considered to be a bizarre event. This belief was strengthened by the nondetection of similar cases over the years with the only exception of the marginal case of DR21. Here, we confirm a similar explosive outflow associated with the UCH_{II} region G5.89−0.39 that indicates that this phenomenon is not unique to Orion or DR21. Sensitive and high angular resolution (∼0.″1) Atacama Large Millimeter/submillimeter Array (ALMA) CO(2−1) and SiO(5−4) observations show that the molecular outflow in the massive star-forming region G5.89−0.39 is indeed an explosive outflow with an age of about 1000 yr and a liberated kinetic energy of 10^{46-49} erg. Our new CO(2−1) ALMA observations revealed over 30 molecular filaments, with Hubble-like expansion motions, pointing to the center of UCH_{II} region. In addition, the SiO(5−4) observations reveal warmer and strong shocks very close to the origin of the explosion, confirming the true nature of the flow. A simple estimation for the occurrence of these explosive events during the formation of the massive stars indicates an event rate of once every ∼100 yr, which is close to the supernovae rate.

Unified Astronomy Thesaurus concepts: Star formation (1569); Aperture synthesis (53); Massive stars (732); Stellar jets (1607); Stellar-interstellar interactions (1576)

Supporting material: animation

1. Introduction

The explosive outflows (with a kinetic energy injected that reaches the 10^{47-49} erg range) are suggested to be powered by the liberation of gravitational energy associated with the formation of a nearby stellar massive binary or maybe a protostellar merger (Bally & Zinnecker 2005; Bally et al. 2017; Zapata et al. 2017). The explosive molecular outflows are composed of tens of narrow straight molecular filament-like ejections with clear Hubble-like velocity increments that point back approximately to a common origin, and with a nearly isotropic configuration (Zapata et al. 2009; Bally et al. 2017, 2020). Rivera-Ortiz et al. (2019) showed that the duration of such explosive outflows should be around some 1000 yr. As more cases like Orion-KL or DR 21 come to light we would know to what extent the dynamical interactions are a key ingredient in order to form massive stars. Sensitive searches using the recently finished Atacama Large Millimeter/submillimeter Array (ALMA) observatory will be very important to discover more explosive outflows and runaway stars in nearby massive star-forming regions.

G5.89−0.39, or W28A2, is a massive star-forming region located at a distance of $2.99^{+0.19}_{-0.17}$ kpc (Sato et al. 2014). This region contains a bright expanding shell-like UCH_{II} region with a dynamical age of 600^{+250}_{-125} yr, estimated from its expansion rate (Acord et al. 1998). Feldt et al. (2003) proposed that a massive young O5 V star, revealed by their near-infrared Nasmyth Adaptive Optics System (NAOS) and the Near-Infrared Imager and Spectrograph CONICA (NACO) at the Very Large Telescope (VLT; NACO-VLT) observations, is energizing the UCH_{II} region. This object, however, is offset by about 1″ to the northwest from the center of the shell-like UCH_{II} region. Feldt et al. (2003) also proposed that the young O5 V star may have migrated from the center of the UCH_{II} region to the present place with a velocity of about 10 km s^{-1} some 1000 yr ago. A second infrared object is also located at the edge of the UCH_{II} region that is called Puga's star (Puga et al. 2006) and is related to a northeast optical outflow. The nature of the molecular outflow in this region is not clear (Zapata et al. 2019). Harvey & Forveille (1988) reported that the molecular outflow located in G5.89−0.39 is one of the most powerful outflows in our Galaxy with a kinetic energy of $\sim 10^{49}$ erg. However, more recent estimations place the energetics of this outflow in a range between 10^{46-48} erg (Acord et al. 1998; Klaassen et al. 2006). Using Chandra observations, Hampton et al. (2016) reported the presence of a gamma-ray source (HESS J1800–240B) associated with G5.89−0.39 that

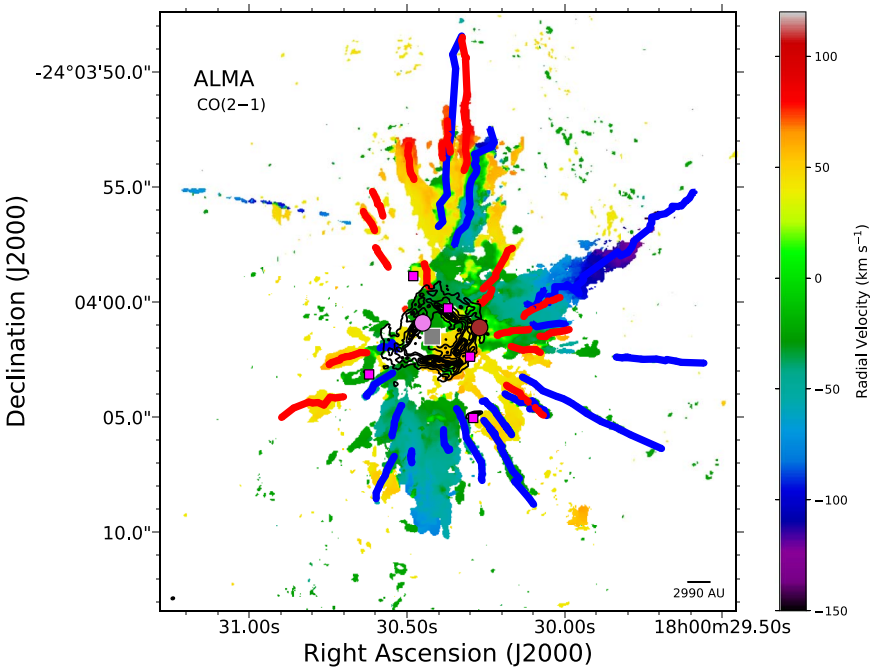

Figure 1. ALMA CO(2−1) moment-one map overlaid with the approaching (blue) and receding (red) explosive filaments in the G5.89−0.39 outflow and the 1.3 mm continuum emission in contours that are tracing the UCH_{II} region in the central part. At these wavelengths emission from UCH_{II} region is still dominated by free–free emission (Hunter et al. 2008). To compute this map, we integrated in radial velocities from −150 to −20 km s^{-1} for the blueshifted emission, while from +40 to +120 km s^{-1} for the redshifted emission. The contours range from 10% to 70% of the peak emission, in steps of 10%. The peak of the millimeter continuum emission is 34 mJy beam^{-1}. The position and velocity of every condensation can be seen in the 3D image presented in Figure 3. The half-power contour of the synthesized beam of the line image is shown in the bottom left corner. The LSR radial-velocity scale-bar (in km s^{-1}) is shown at the right. In the bottom right corner is also shown the spatial scale at a distance of 2.99 kpc. The locations of the sources named Feldt's star (Feldt et al. 2003; pink circle) and Puga's star (Puga et al. 2006; brown circle) are shown at the center of the explosive outflow. The magenta squares mark the location of the objects reported with the SMA (Hunter et al. 2008). The gray square marks the origin of the outflow.

may be related to the outflow arising from here. Very recently, Zapata et al. (2019), using Submillimeter Array (SMA) observations, detected the presence of six explosive filaments pointing directly to the center of the UCH_{II} region. They deduced the presence of an explosive outflow and suggested a relation between the UCH_{II} region and the flow, but their study was not conclusive.

Here, using much more sensitive[12] spectral line ALMA CO(2−1) and SiO(5−4) observations together with a much better beam area[13] provided us a better fidelity in the spectral and continuum images to study in more detail the intriguing molecular outflow in G5.89−0.39.

2. Observations

The ALMA observations of G5.89−0.39 were carried out in 2019 September 5 as part of the Cycle 6 program 2018.1.00513.S (PI: Paul Ho). These observations were split in two sessions, one with 49 antennas and the other with 45 antennas, both using antennas with diameters of 12 m, yielding baselines with projected lengths from 38 to 3600 m (29–2769 $k\lambda$). As the primary beam at this frequency (Band 6) has an FWHM of about 25″, the outflow from G5.89−0.39 was covered with a single pointing at the sky position $\alpha_{J2000.0} = 18^h00^m30\overset{s}{.}388$, and $\delta_{J2000.0} = -24°04'00\overset{''}{.}20$. The total integration time on source that includes the two sessions is 78 minutes. The maximum recoverable scale for these observations is 2.″5.

The weather conditions were excellent during these observations, with an average system temperature around 90 K and with an average precipitable water vapor around 1.8 mm. During these observations, the 183 GHz water line was monitored with water vapor radiometers (WVRs), used to reduce atmospheric phase fluctuations. The quasars J1924−2914, J1820−2528, and J1831−2714 were used as the amplitude, atmosphere, bandpass, pointing, gain fluctuations, and WVR calibrators.

The continuum image presented in Figure 1 was obtained by averaging line-free spectral channels of nine spectral windows. The total bandwidth for the continuum is about 3.75 GHz. The spectral windows were selected to observe different molecular lines as for example CH_3OH, HC_3N, CO, and SiO. In this Letter, we concentrate on the emission of the SiO(5−4) and CO(2−1) spectral lines at rest frequencies of 217.105 and 230.538 GHz, respectively. An in-depth study for the rest of the lines will be presented in a future paper. The spectral windows where we detected the SiO and CO have a native channel spacing of 488.3 kHz or ∼0.61 km s^{-1}. However, given the broad velocity range of the lines, we smoothed the spacing channel to 2.44 km s^{-1}.

The data were calibrated, imaged, and analyzed using the Common Astronomy Software Applications (CASA) package, Version 5.6 (McMullin et al. 2007). We also used some routines in Python to image the data (Astropy Collaboration et al. 2013). We imaged the *uv*-data using the task TCLEAN. We set the `Robust` parameter of TCLEAN equal to 0.5 for the continuum and line emissions. We obtained an image rms-noise for the 1.3 mm continuum of 0.2 mJy beam^{-1} at an

[12] A factor of 40 better in the rms noises, compared with the previous SMA observations (Zapata et al. 2019).
[13] Almost a factor of 70, again compared with the previous SMA observations.

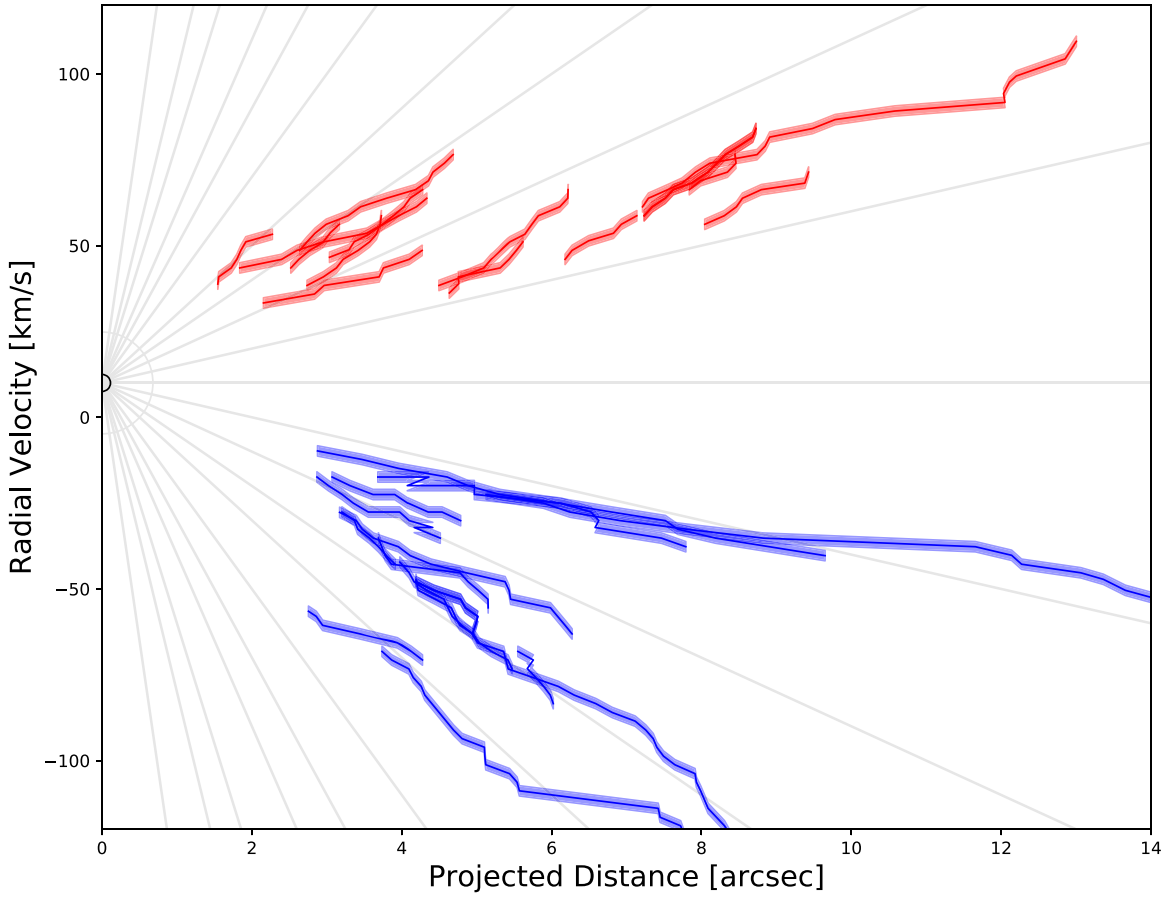

Figure 2. Position–velocity diagram of the explosive CO(2−1) filaments in the G5.89−0.39 outflow found with the present ALMA observations. Here, we have only included the maximum velocities in a range between ±120 km s^{-1}; there are some molecular filaments that extend outside of this window as can be noted in Figure 1. We have colored the approaching filaments in blue, and the receding ones in red. In each filament the shaded blue and red colors represent the error area that is about 0.″1 for the on-the-sky distance, and 1.2 km s^{-1} for the radial velocity. As in the Orion BN-KL and DR21 explosive outflows, all velocities vary linearly with distance with no clear deceleration. Almost all filaments seem to converge to a systemic velocity range +12 to −10 km s^{-1}. The cloud velocity of most of the detected molecular lines is around 9 km s^{-1} (Hunter et al. 2008; Su et al. 2009). All gray lines begin at R = 0 and a radial velocity of 0 km s^{-1}.

angular resolution of 0.″12 × 0.″09 with a position angle (PA) of −75°. The ALMA theoretical rms-noise for this configuration, integration time, bandwidth, and frequency is approximately 0.02 mJy beam^{-1}, which is an order of magnitude smaller. The strong continuum emission from the UCH$_{II}$ region (with a density flux of about 10 Jy and a dynamic range of 200) did not allow us to reach the theoretical noise levels. An alternative possibility is the lack of short spacing information on the continuum structure.

The line-image rms-noise is 0.75 mJy beam^{-1} km s^{-1} at an angular resolution of 0.″13 × 0.″09 with a PA of −73°. The ALMA theoretical rms-noise for this configuration, integration time, bandwidth (channel spacing), and frequency is about 0.7 mJy beam^{-1}, which is also very close to the value we obtain in the line images. It is interesting to note that even when the line sensitivity is very close to that obtained theoretically, for the continuum emission it is not the case, again suggesting that the bright emission from the UCH$_{II}$ region is responsible for the increased rms-noise.

Phase self-calibration was done using the continuum emission as a model, and then we applied the solutions to the line emission. We obtained about a factor 2 improvement in the rms-noise.

3. Results and Discussion

In Figure 1 we present the CO(2−1) moment-one map (intensity-weighted velocity image), traditionally used to obtain the "velocity field," overlaid with the 1.3 mm continuum emission, and the 34 expanding filaments reported here that are related with this outflow. This map may help the reader to see clearly the expanding filaments emerging from the center of the flow. This thermal emission was especially selected from outside the velocity range from −20 to +40 km s^{-1}, where the emission arises from the systemic molecular cloud and probably from some other clouds along the line of sight. At these velocities there are also strong absorption features associated with the UCH$_{II}$ at the center of the flow. We avoid here the confusing emission close to the embedding cloud systemic velocity, rather focusing on the filaments at higher velocities. The CO(2−1) thermal emission is found from −170 up to +130 km s^{-1}. These velocities are broader as compared to those radial velocities reported in recent SMA studies (Hunter et al. 2008; Su et al. 2012; Zapata et al. 2019), probably because the better ALMA sensitivity allows us to detect fainter emission at higher velocities. We find 17 blueshifted and 17 redshifted expanding filaments emerging from G5.89−0.39. Each filament marks the position of one

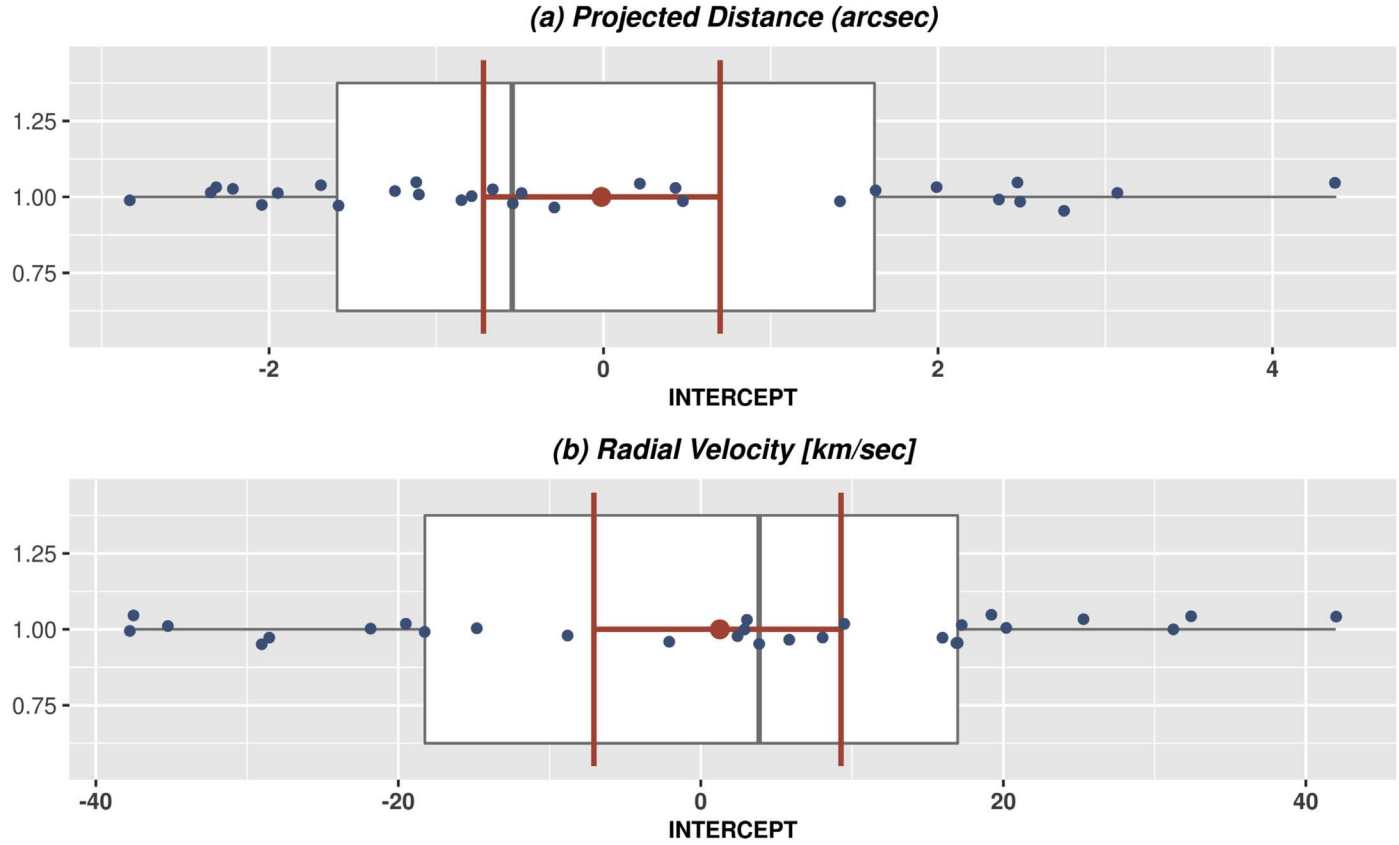

Figure 3. 95% intercept estimates confidence intervals (red lines) for the projected distance (a) with a statistical error of $0\farcs7421$, and radial velocity (b) with a statistical error of 8.5129 km s^{-1}. The blue points represent the jittered intercept estimated points. Relative origin (0,0) belongs to each interval with the *p*-value estimated to be 0.9725 and 0.7643. The gray line and the red dot represent the median and mean values, respectively.

sequence of molecular condensations mapped at different spectral channel velocities, as already done in this Letter, and other massive star-forming regions (Zapata et al. 2009, 2013, 2019). These filaments coincide very well with some filamentary structures already traced by the moment-one map and the six explosive filaments reported in Zapata et al. (2019). The most prominent filaments in Figure 1, the three blueshifted to the south/north of the explosive event and the two redshifted to the north, are the ones already reported by those SMA observations (Hunter et al. 2008; Su et al. 2012; Zapata et al. 2019). The rest of the filaments are new detections and give a more complete view of the explosiveness of the flow in G5.89−0.39.

In Figure 1, it is also clear that the filaments get bluer or redder with increasing projected distance from their origin, suggesting that they follow a Hubble-velocity law, that is, the velocities increase linearly with on-the-sky distance from the center. This phenomenon is confirmed in the position–velocity diagram obtained in Figure 2. This property is one of the main features that characterize the explosive outflows (Zapata et al. 2017). In Figure 1, the 1.3 mm continuum contours delineate a shell-like structure that is associated with the expanding and ionized UCH$_{\rm II}$ region reported in G5.89−0.39 (Wood & Churchwell 1989; Acord et al. 1998; Hunter et al. 2008). All filaments converge to the center of the UCH$_{\rm II}$, the place where they originated. This position is located at $\alpha_{\rm J2000.0} = 18^{\rm h}00^{\rm m}30\fs42 \pm 0.005^{\rm s}$ and $\delta_{\rm J2000.0} = -24\arcdeg04\arcmin01\farcs5 \pm 0\farcs75$. The position given here is similar to the one obtained in Zapata et al. (2019) for the convergence of the six molecular filaments, but now with a better error. In addition, we also include in this figure the positions of the two objects located in the vicinities of the ionized shell, the Feldt et al. (2003) and Puga et al. (2006) objects reported at infrared wavelengths. In this figure, we mark the location of the dusty and compact objects reported by the SMA observations (Hunter et al. 2008). Massive young stars found in the periphery of the UCH$_{\rm II}$ region are likely related to the energetic explosion, but an in-depth proper motion study at optical or maybe infrared wavelengths is necessary to search for runaway massive stars in this region, as in the case of Orion BN-KL (Rodríguez et al. 2020). A search for an optical counterpart of the Feldt's star in the GAIA catalog failed (Zapata et al. 2019), likely because of the high extinction at low galactic latitudes (Foster et al. 2012).

In Figure 2, we present the on-the-sky distance versus the radial-velocity plot of the 34 expanding filaments reported in this Letter, and presented in the moment-one map (Figure 1). As mentioned earlier, the filaments follow nearly straight lines and seem to converge to a radial-velocity range between −7.2 and +9.7 km s^{-1}, and the systemic velocity of the molecular cloud in G5.89−0.39 is around 9 km s^{-1}; see Figure 7 from Hunter et al. (2008). In all filaments the radial velocities increase linearly with the projected distance to the center of the UCH$_{\rm II}$ region, that is, follow a clear Hubble-velocity law. This pattern was already revealed by the SMA observations for the six filaments (Zapata et al. 2019), but it was not completely demonstrated that they indeed belonged to an explosive outflow. The lack of deceleration in the filaments is an indication of the impulsive nature of the expansion. This implies that the density of the ejecta must be substantially larger than the medium through which they move. In a Hubble

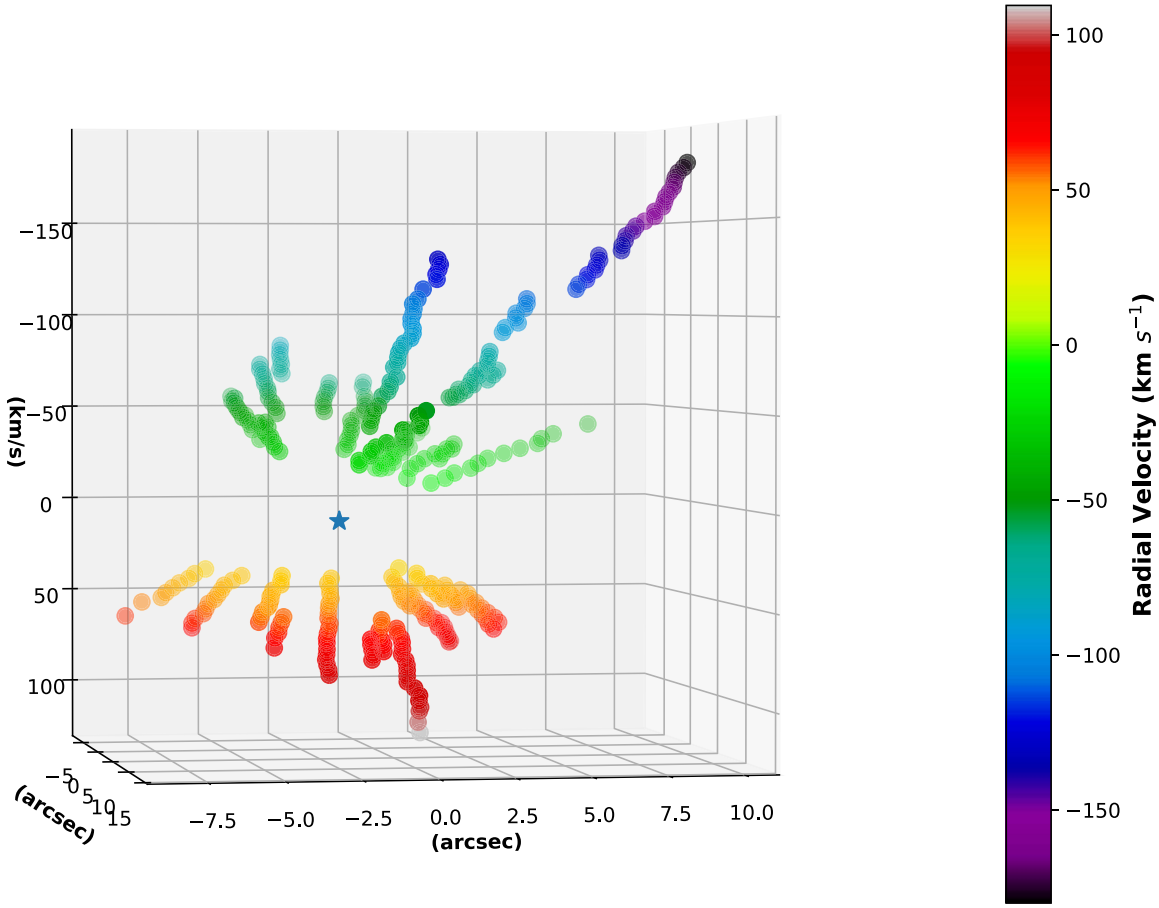

Figure 4. Three-dimensional animation of the explosive event in G5.89−0.39. The radial blueshifted and redshifted velocities are shown from blue to red colors. The LSR radial-velocity scale-bar (in km s^{-1}) is shown at the right. The (0″, 0″, 0 km s^{-1}) position is the origin. The star marks the position of the explosive outflow origin. The animation starts with a view from up to down and then left to right. The duration of the animation is about 10 s.

(An animation of this figure is available.)

flow created by an explosion about 1000 yr ago, slower ejecta have moved a smaller distance than faster ejecta, which has moved farther.

In Figure 3, we present a statistical analysis on the origin of the explosive outflow in G5.89. In this figure is shown the jittered intercept estimated points and mean interval confidence for intercepts. Removing three outlier trajectories (or filaments), the mean of the projected distance intercepts is $\bar{x} = -0\farcs01$ and a 95% confidence interval for the mean of intercepts is IC$_\mu$ = (−0.″75, 0.″73). The radial-velocity mean of intercepts is $\bar{x} = +1.26$ km s^{-1}, and a 95% confidence interval for the mean of intercepts is IC$_\mu$ = (−7.25 km s^{-1}, 9.77 km s^{-1}). With p-value of 0.9725 for the projected distance and p-value of 0.7643 for the radial velocity the hypothesis of $\mu = 0$ cannot be rejected for both cases. These results show that statistically all trajectories have a common coordinated system origin. We included this origin in Figure 1.

The fact that the filaments are not straight lines reveals internal structure, probably because of lateral or across-the-line-of-sight motions. From these discrepancies, we can estimate the linear dispersion across the filaments, assuming a displacement of about 1″ away from a linear trajectory over 1000 yr, implies a traverse velocity of about 15 km s^{-1}. Alternatively, these displacements may result from deflection of the ejecta by dense clumps. From the position–velocity diagram, taking the maximum radial velocity of about 160 km s^{-1} and the maximum projected distance of 12″, we obtained a kinematic age of 1000 yr, a similar value for the fossil outflow reported by Klaassen et al. (2006) and the estimated time to reach the present position of the Feldt's star.

A three-dimensional (3D) view of the explosive outflow is presented in Figure 4. This image has three axes, the projected distance in R.A. and decl. (in arcseconds), and the radial velocity (in km s^{-1}) of the filaments. Here, the central position is at (0″, 0″, +0 km s^{-1}), where in R.A. it is at 18$^{\rm h}$00$^{\rm m}$30$^{\rm s}$.42 and decl. it is at −24°04′01.″5. In the figure it is clearly seen how the colors/velocities change getting bluer or redder far from the origin indicating a Hubble-law velocity of each filament as already noted. It is important to mention that inside of the UCH$_{\rm II}$ region there is no emission from the filaments, and they appear to start a bit farther from this position; see Figure 2.

In Figure 5 the moments of order zero (upper panel) and one (lower panel) emission of the SiO(5−4) spectral line from G5.89 −0.39 are presented. To make this figure, we integrated from −50 to +50 km s^{-1} in radial velocities. This velocity range includes the radial velocities close to the systemic cloud velocities (+9 km s^{-1}), but as this molecule emission is found mainly in strong shocks (Schilke et al. 1997), ALMA could sample very well all these velocities, with no ambient cloud contamination. We resolved the SiO thermal emission, and revealed many filaments in almost every orientation (i.e., with a nearly isotropic orientation), and again pointed back to the center of the UCH$_{\rm II}$ region. Overall the SiO maps confirm the explosion in this region. Only a few SiO

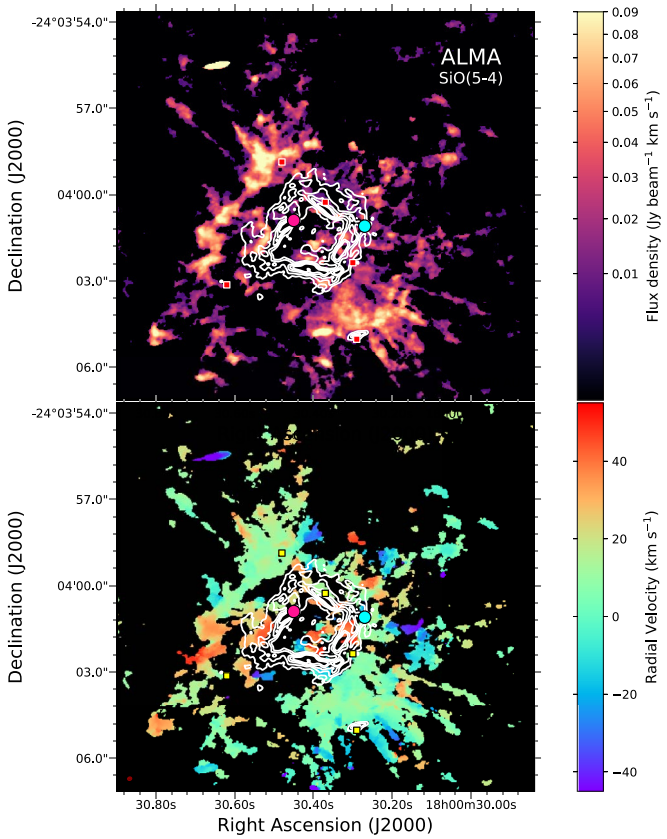

Figure 5. ALMA SiO(5-4) moment-zero (upper panel) and moment-one (lower panel) overlaid with the 1.3 mm continuum emission in white contours that are tracing the UCH_{II} region. The contours range from 10% to 70% of the peak emission, in steps of 10%. The peak of the millimeter continuum emission is 34 mJy beam^{-1}. To compute these maps, we integrated in radial velocities from −50 to +50 km s^{-1}. The half-power contour of the synthesized beam of the line image is shown in the bottom left corner of the lower panel. The LSR radial-velocity scale-bar (in km s^{-1}) is shown at the right of the lower panel. The location of the sources named Feldt's star (Feldt et al. 2003) (pink circle) and Puga's star (Puga et al. 2006) (cyan circle) are shown at the center of the explosive outflow. The magenta squares mark the location of the objects reported with the SMA (Hunter et al. 2008). All SMA objects have an ALMA counterpart, but this discussion is outside of the scope of this Letter.

filaments have a counterpart in the CO emission. Most of the CO filaments are found farther out from the SiO ones, and with broader velocity ranges. The northwest bipolarity reported for this SiO outflow (Acord et al. 1998; Sollins et al. 2004) is totally lost in these new ALMA images, in which the outflow is more resemblant of an explosion.

Finally, one can make a very crude estimation of the rate of the explosive outflows occurring in our Galaxy using the cases of Orion BN/KL, DR21, and G5.89−0.39. If we assume that this event occurs approximately three times every 10,000 yr (the kinematic age of DR21) in a radius of 2.99 kpc, we obtain a rate of about one explosion every 130 yr, close to the rate of supernovae (Tammann et al. 1994). The similarity between the event rates of explosive protostellar outflows and supernovae suggests that stellar dynamical interactions may play important roles in the formation of massive stars. Models of high-mass star formation should be revised to include dynamical interactions.

4. Conclusions

In summary, the sensitive and high angular ALMA observations allow us to find that the outflow in G5.89−0.39 is indeed an explosion that emerged from the center of an ionized UCH_{II} region, and where young massive stars placed in its periphery could have powered the flow, but they moved from the center. G5.89−0.39 is thus the third explosive outflow in the Galaxy until now. Dedicated searches for explosive outflows in nearby massive star-forming regions (for instance, if they take place when a protostellar merger is produced or by the formation of a capture of a companion into a close binary orbit) could show this phenomenon to be more common than previously thought.

We would like to thank the anonymous referee for the thoughtful suggestions that helped to improve our manuscript. This Letter makes use of the following ALMA data: ADS/JAO.ALMA#2018.1.00513.S. ALMA is a partnership of ESO (representing its member states), NSF (USA) and NINS (Japan), together with NRC (Canada), MOST and ASIAA (Taiwan), and KASI (Republic of Korea), in cooperation with the Republic of Chile. The Joint ALMA Observatory is operated by ESO, AUI/NRAO and NAOJ. The National Radio Astronomy Observatory is a facility of the National Science Foundation operated under cooperative agreement by Associated Universities, Inc. L.F.R. is grateful to CONACyT, México, and DGAPA, UNAM for the financial support. L.A.Z. acknowledges financial support from CONACyT-280775 and UNAM-PAPIIT IN110618 grants, México. A.P. acknowledges financial support from CONACyT and UNAM-PAPIIT IN113119 grant, México. P.T.P.H. acknowledges financial support from MOST 108-2112-M-001-016-MY1. P.S. was partially supported by a Grant-in-Aid for Scientific Research (KAKENHI No. 18H01259) of the Japan Society for the Promotion of Science (JSPS). P.R.R.-O. acknowledges funding from the European Research Council (ERC) under the European Union's Horizon 2020 research and innovation program, for the Project "The Dawn of Organic Chemistry" (DOC), grant agreement No. 741002.

Facility: ALMA.

Software: CASA (McMullin et al. 2007), KARMA (Gooch 1996).

ORCID iDs

Luis A. Zapata https://orcid.org/0000-0003-2343-7937
Paul T. P. Ho https://orcid.org/0000-0002-3412-4306
Manuel Fernández-López https://orcid.org/0000-0001-5811-0454
Luis F. Rodríguez https://orcid.org/0000-0003-2737-5681
John Bally https://orcid.org/0000-0001-8135-6612
Aina Palau https://orcid.org/0000-0002-9569-9234
Masao Saito https://orcid.org/0000-0003-0769-8627
Patricio Sanhueza https://orcid.org/0000-0002-7125-7685
P. R. Rivera-Ortiz https://orcid.org/0000-0001-6867-4210
A. Rodríguez-González https://orcid.org/0000-0002-2606-8527

References

Acord, J. M., Churchwell, E., & Wood, D. O. S. 1998, ApJL, 495, L107
Astropy Collaboration, Robitaille, T. P., Tollerud, E. J., et al. 2013, A&A, 558, A33
Bally, J., Ginsburg, A., Arce, H., et al. 2017, ApJ, 837, 60
Bally, J., Ginsburg, A., Forbrich, J., et al. 2020, ApJ, 889, 178
Bally, J., & Zinnecker, H. 2005, AJ, 129, 2281
Feldt, M., Puga, E., Lenzen, R., et al. 2003, ApJL, 599, L91
Foster, J. B., Stead, J. J., Benjamin, R. A., et al. 2012, ApJ, 751, 157

Gooch, R. 1996, in ASP Conf. Ser. 101, Astronomical Data Analysis Software and Systems V, ed. G. H. Jacoby & J. Barnes (San Francisco, CA: ASP), 80
Hampton, E. J., Rowell, G., Hofmann, W., et al. 2016, JHEAp, 11, 1
Harvey, P. M., & Forveille, T. 1988, A&A, 197, L19
Hunter, T. R., Brogan, C. L., Indebetouw, R., & Cyganowski, C. J. 2008, ApJ, 680, 1271
Klaassen, P. D., Plume, R., Ouyed, R., et al. 2006, ApJ, 648, 1079
McMullin, J. P., Waters, B., Schiebel, D., Young, W., & Golap, K. 2007, in ASP Conf. Ser. 376, Astronomical Data Analysis Software and Systems XVI, ed. R. A. Shaw, F. Hill, & D. J. Bell (San Francisco, CA: ASP), 127
Puga, E., Feldt, M., Alvarez, C., et al. 2006, ApJL, 641, 373
Rivera-Ortiz, P. R., Rodríguez-González, A., Hernández-Martínez, L., et al. 2019, ApJ, 885, 104
Rodríguez, L. F., Dzib, S. A., Zapata, L., et al. 2020, ApJ, 892, 82
Sato, M., Wu, Y. W., Immer, K., et al. 2014, ApJ, 793, 72
Schilke, P., Walmsley, C. M., Pineau des Forets, G., et al. 1997, A&A, 321, 293
Sollins, P. K., Hunter, T. R., Battat, J., et al. 2004, ApJL, 616, L35
Su, Y.-N., Liu, S.-Y., Chen, H.-R., et al. 2012, ApJL, 744, L26
Su, Y.-N., Liu, S.-Y., Wang, K.-S., et al. 2009, ApJL, 704, L5
Tammann, G. A., Loeffler, W., & Schroeder, A. 1994, ApJS, 92, 487
Wood, D. O. S., & Churchwell, E. 1989, ApJS, 69, 831
Zapata, L. A., Ho, P. T. P., Guzmán Ccolque, E., et al. 2019, MNRAS, 486, L15
Zapata, L. A., Schmid-Burgk, J., Ho, P. T. P., et al. 2009, ApJL, 704, L45
Zapata, L. A., Schmid-Burgk, J., Pérez-Goytia, N., et al. 2013, ApJL, 765 L29
Zapata, L. A., Schmid-Burgk, J., Rodríguez, L. F., et al. 2017, ApJ, 836, 133